Proceedings of ASME Turbo Expo 2017: Turbomachinery Technical Conference and Exposition
GT2017
June 26-30, 2017, Charlotte, North Carolina, USA

GT2017-63692

THE EFFECT OF AREA RATIO CHANGE VIA INCREASED HOLE LENGTH FOR SHAPED FILM COOLING HOLES WITH CONSTANT EXPANSION ANGLES

Shane Haydt
Stephen Lynch
Mechanical and Nuclear Engineering Department
The Pennsylvania State University
University Park, PA, USA

Scott Lewis
Turbine Durability
United Technologies—Pratt & Whitney
400 Main Street
East Hartford, CT 06108, USA

ABSTRACT

Shaped film cooling holes are used as a cooling technology in gas turbines to reduce metal temperatures and improve durability, and they generally consist of a small metering section connected to a diffuser that expands in one or more directions. The area ratio of these holes is defined as the area at the exit of the diffuser, divided by the area at the metering section. A larger area ratio increases the diffusion of the coolant momentum, leading to lower average momentum of the coolant jet at the exit of the hole and generally better cooling performance. Cooling holes with larger area ratios are also more tolerant of high blowing ratio conditions, and the increased coolant diffusion typically better prevents jet liftoff from occurring. Higher area ratios have traditionally been accomplished by increasing the expansion angle of the diffuser while keeping the overall length of the hole constant. The present study maintains the diffuser expansion angles and instead increases the length of the diffuser, which results in longer holes. Various area ratios have been examined for two shaped holes: one with forward and lateral expansion angles of 7° (7-7-7 hole) and one with forward and lateral expansion angles of 12° (12-12-12 hole). Each hole shape was tested at numerous blowing ratios to capture trends across various flow rates. Adiabatic effectiveness measurements indicate that for the baseline 7-7-7 hole, a larger area ratio provides higher effectiveness, especially at higher blowing ratios. Measurements also indicate that for the 12-12-12 hole, a larger area ratio performs better at high blowing ratios but the hole experiences ingestion at low blowing ratios. Steady RANS simulations did not accurately predict the levels of adiabatic effectiveness, but did predict the trend of improving effectiveness with increasing area ratio for both hole shapes. Flowfield measurements with PIV were also performed at one downstream plane for a low and high area ratio case, and the results indicate an expected decrease in jet velocity due to a larger diffuser.

INTRODUCTION

Film cooling holes are a technology used in gas turbines to reduce the metal temperature and increase the durability of hot gas path components. Film cooling holes are drilled into the surface of these components, and coolant is ejected out of them to create a film over the surface. The addition of a diffuser to the outlet of a cylindrical hole is advantageous for film cooling performance [2]. The diffuser decreases the momentum of the coolant jet, decreases the ejection angle, and spreads the coolant laterally. Many parameters of the diffuser have been varied in order to find optimal performance.

Some of those parameters are depicted in Figure 1. The shape and size of a diffuser are determined by its length (L_{diff}/D), forward expansion angle (β_{fwd}), and lateral expansion angle (β_{lat}). An increase in these parameters results in a larger diffuser, the size of which can be defined by the area ratio (AR). AR is the ratio between the area at the exit plane of the diffuser and the area at the metering section, or cylindrical inlet of the hole, measured normal to the centerline of the cooling hole. By mass conservation, a larger area ratio results in a lower average velocity of the coolant jet as it leaves the hole.

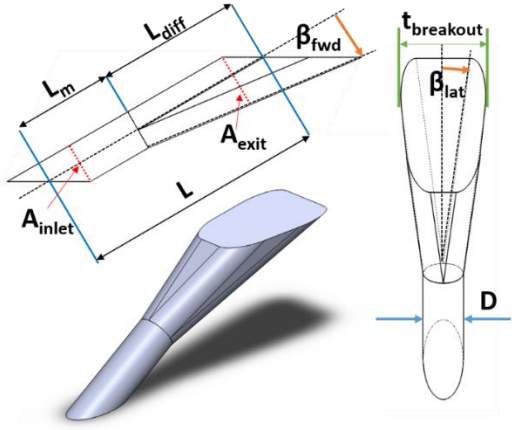

Figure 1: 7-7-7 baseline shaped film cooling hole, developed by Schroeder and Thole [1].

Traditionally, area ratio has been increased by increasing the expansion angles of the diffuser. The L/D of the hole is generally unchanged by this variation in area ratio, and in literature it tends to fall in the range of 2 < L/D < 10. For the present study, the expansion angles were maintained and the L/D of the diffuser was changed in order to vary AR from 2 to 6. This isolates the effect of increasing area ratio from the effect of expansion angle.

Designers, manufacturers, and academics could benefit from a deeper understanding of the impact of area ratio on film cooling performance, beyond the range of what has traditionally been studied. This type of understanding might be applied to optimize the cooling in a region of a turbomachinery component that has a sufficiently thick wall to enable an optimally larger diffuser. Some examples of such regions where ample wall thickness often exists for potentially large film hole diffusers include a turbine blade platform or the lower (0-50%) spans of a turbine blade airfoil.

NOMENCLATURE

A	hole cross-sectional area
AR	area ratio, A_{exit}/A_{inlet}
c_f	skin friction coefficient
D	diameter of film cooling holes
DR	density ratio, ρ_c/ρ_∞
H	shape factor, δ^*/θ
I	momentum flux ratio, $\rho_c U_c^2/\rho_\infty U_\infty^2$
k	thermal conductivity
L	hole length
$\dot{m}_c$	coolant mass flow rate
M	blowing ratio, $\rho_c U_c/\rho_\infty U_\infty$
P	pitch, lateral distance between holes
Re	Reynolds number ($Re^* = \delta * u_\tau/\nu_\infty$, $Re_\theta = U_\infty * \theta/\nu_\infty$, $Re_D = U_\infty * D/\nu_\infty$, $Re_c = U_c * D/\nu_c$)
t	hole breakout width
T	temperature
Tu	freestream turbulence intensity, u_{rms}/U_∞
U_∞	mainstream mean velocity
u_{jet}	coolant jet velocity in the direction of the metering section centerline
u_{rms}	root mean squared velocity
u_τ	friction velocity, $U_\infty\sqrt{c_f/2}$
V	velocity magnitude
x	downstream distance measured from hole trailing edge
y	vertical distance from surface
z	spanwise distance measured from center hole

Greek

α	hole injection angle
β	expansion angle for diffuser
δ	99% boundary layer thickness
δη	experimental uncertainty in effectiveness
$\delta\eta_b$	bias uncertainty in effectiveness
δ^*	displacement thickness
η	local adiabatic effectiveness, $(T_\infty - T_{aw})/(T_\infty - T_c)$
θ	momentum thickness
ν	kinematic viscosity
ρ	fluid density
φ	non-dimensional fluid temperature, $(T_\infty - T)/(T_\infty - T_c)$

Subscripts

aw	adiabatic wall
c	coolant, at hole inlet
CL	centerline
eff	effective, at hole exit
exit	exit plane of the film cooling hole
fwd	forward expansion of diffuser
inlet	inlet plane of the film cooling hole
lat	lateral expansion of the diffuser
m	metering section
∞	mainstream

Superscripts

¯	laterally-averaged
=	area-averaged

REVIEW OF RELEVANT LITERATURE

Shaped film cooling holes have been an important area of focus since the seminal study by Goldstein et al. [3] showed that they provide higher adiabatic effectiveness than cylindrical holes, especially at high blowing ratios. As outlined in the review of shaped hole literature by Bunker [2], the advantage of a shaped film cooling hole is that it reduces the momentum of the fluid while providing a wider surface coverage. A shaped hole that is laterally and/or forwardly expanded has reduced jet penetration into the mainstream, reduced velocity gradients, and reduced turbulence production downstream, as shown by Thole et al. [4].

A canonical feature of all film cooling holes is the counter-rotating vortex pair (CRVP), which was show by Peterson [5] to be formed by the shear layer between the coolant jet and the mainstream flow. If the strength of the shear layer is reduced, for example by reducing the momentum of the coolant jet, the strength of the CRVP is also reduced [2]. The CRVP promotes jet lift-off and entrainment of the mainstream flow towards the wall, and thus reducing the strength of the CRVP is a primary motivation for film cooling research [2]. Shaped holes with a large breakout width can also have a secondary feature called "anti-kidney vortices" which counteract the detrimental effects of the CRVP, as shown by Haven et al. [6]. The vorticity created by the hole's leading edge boundary layer is initially aligned normal to the streamwise flow direction, but is realigned in the streamwise direction by entrainment of the mainstream flow [6]. This vorticity creates intermittent "anti-kidney vortices", so-named because they act in opposition to the CRVP, also known as "kidney vortices".

Film cooling geometry design parameters can have a profound effect on film cooling effectiveness, and this has been a focus of much of the film cooling research for the past few decades. Gritsch et al. [7] examined 14 film cooling hole variations in order to isolate the effect of several parameters: L/D, P/D, t/P, and AR. They found that changing the L/D of shaped holes has a negligible effect on $\bar{\eta}$, if AR and t/P remain constant. Also, $\bar{\eta}$ increases with decreasing P/D, which is expected since the holes are spaced more closely together, but

when $\bar{\eta}$ is normalized by P/D, it was found that for low P/D the holes are too close to make efficient use of coolant per unit span. The coverage ratio, t/P, has little to no effect at low blowing ratios, but at high blowing ratios, the increased lateral diffusion due to higher t/P leads to higher $\bar{\eta}$. Finally, Gritsch et al. found that when t/P remained constant, AR had no effect on $\bar{\eta}$, for the range of AR=3.5-4.7.

Another study by Saumweber and Schulz [8] showed the effect of the expansion angle, inclination angle, and meter length parameters. The effects of these parameters were negligible at low blowing ratios, but more significant at high blowing ratios. Decreasing inclination angle from 60°-30° and increasing expansion angle from 6°-14° lead to increased η. Increasing the metering section length slightly decreased η primarily at high M.

Using the previously mentioned data sets, among others, Colban et al. [9] determined a shaped film cooling hole correlation using the parameters thought to be most important to the effectiveness: AR, P/D, M, t/P, and distance downstream. This correlation agreed well with data sets representing film cooling holes with AR/(M*P/D)=0.17-1.17, t/P=0.31-0.65, and M=0.2-2.5.

It is important to note that in these aforementioned data sets, higher area ratios were achieved by increasing the forward and lateral expansion angles of the diffuser while maintaining the overall length of the film cooling hole. Therefore, the area ratio effect is not isolated, but conflated with the effect of expansion angle, and high area ratios were not achieved without prohibitively high expansion angles. Kohli and Bogard [10] and Thole et al. [4] have shown that if the expansion angle of a hole is too high, it can be detrimental to film cooling performance. At large expansion angles, separation can occur within the hole, which can cause higher turbulence levels at the hole outlet and also mainstream ingestion into the diffuser, both of which would reduce the performance of the jet [4, 10].

Saumweber and Schulz [8] also noted a bimodal effectiveness pattern for holes with large expansion angles. From computation studies, such as Kohli and Thole [11], the existence of a separation region on the downstream wall of the diffuser is well-established. The spatial extent of the separation bubble is increased by increasing expansion, and thus the displacement of fluid towards the sidewalls is also increased. This velocity deficit is maintained downstream, occasionally creating a bimodal effectiveness pattern in extreme cases.

To help explain the complicated parameter effects of a film cooling diffuser, it is instructive to learn from the well-established understanding of ideal conical diffusers. McDonald and Fox [12] investigated the pressure recovery and efficiency of conical diffusers of varying shapes and sizes. This study found that the pressure recovery and diffuser effectiveness scale with the cone half angle and the ratio between diffuser length and radius. Long and narrow diffusers with moderate cone half angles have the best pressure recovery, the analogous film cooling hole case being a hole with a long L-L_m and a moderate lateral and forward expansion angle.

There are several notable differences between classical conical diffuser studies and a film cooling hole diffuser, primarily in the nonuniform inlet and outlet conditions experienced by a film hole. Klein [13] showed the strong influence that some inlet effects had on the pressure recovery, including an increase in pressure recovery for higher turbulence intensities. However, all velocity inlet profiles in that study were uniform, and there was free discharge at the outlet. Wolf and Johnston [14] examined the effect of non-uniform velocity profiles and their effect on diffuser performance. It was found that diffusers with velocity profiles having a low velocity core-flow region near a wall had decreased pressure recovery as compared to a diffuser with uniform inlet conditions. Additionally, separation occurred at a lower value of AR (with fixed length to radius ratio) for these cases. This type of inlet velocity profile is more consistent with film cooling holes, due to the well-known separation region created in the metering section inlet.

Leylek and Zerkle [15] computationally showed this separation region, which occurs when the coolant goes through a large turning angle from a quiescent plenum. The separation at the inlet leads to a jetting effect of the coolant on the opposite side of the meter section. This leads to the non-uniform velocity profile as described above. This separation region is also a feature of film cooling holes fed by crossflow, as shown by Thole et al. [16] and Saumweber and Schulz [17]. With moderate in-line crossflow, the separation region on the downstream side of the meter inlet can be reduced, but with higher crossflow, the separation region appears on the upstream side of the inlet [16]. Likewise, if the coolant has to undergo the large turning angle on the side of the inlet, due to crossflow, a separation region is created and jetting occurs on the opposite side of the meter [17]. The separation region at the inlet, and the ensuing skewed velocity profile, was also observed experimentally inside a film hole by Coletti et al. [18] using magnetic resonance imaging (MRI).

The in-hole understanding described in this section, and in the current study, are provided primarily by computational fluid dynamics (CFD) predictions. Aside from the aforementioned MRI technique, it is difficult to achieve in-hole pressure or velocity measurements. Haydt et al. [19] showed that the steady RANS realizable k-ε turbulence model was not able to accurately capture the exact levels of effectiveness, but was able to predict flow features in the hole that physically explained the trends of the experimental data.

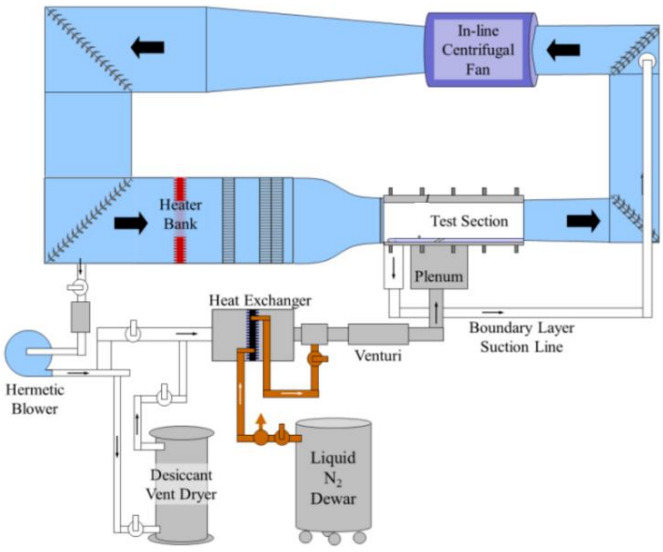

Figure 2. Schematic of the wind tunnel facility used in the current

EXPERIMENTAL FACILITY

A schematic of the wind tunnel facility used for the measurements in this study is shown in Figure 2. This closed-loop wind tunnel has a high temperature, low density mainstream loop and a low temperature, high density coolant loop, both with air as the working fluid. The mainstream flow is held uniform at room temperature using a bank of electrical heating elements and a chilled water heat exchanger, and flow is kept at 10 m/s by an axial fan, with velocity measured by a Pitot probe. As the flow enters the test section, a suction loop removes the incoming mainstream boundary layer, and a new boundary layer develops on the Styrofoam endwall and is transitioned to turbulence by a trip wire located at x/D = -35. Boundary layer measurements for this test section were measured and reported by Schroeder and Thole [1] at low freestream turbulence of Tu = 0.5%. The turbulent boundary layer was measured at x/D = -4.7, and for at least five pitchwise locations. The average values were reported as $\theta/D = 0.14$, $H = 1.45$, $Re_\theta = 670$, $Re^* = 315$, Re_D=4,300, Re_c=5,000-30,000, and $u_\tau = 0.5$ m/s [1].

Flow for the secondary coolant loop is diverted from the mainstream flow by a hermetically sealed blower. The temperature of the coolant flow is lowered in a heat exchanger with liquid nitrogen, and then the gaseous nitrogen exiting the heat exchanger is also added to the flow. In order to avoid frost formation at these cryogenic temperatures, the air is first routed through a vent dryer filled with solid desiccant. Downstream of the heat exchanger and the re-injection of the gaseous nitrogen, the total coolant flow rate is measured by a venturi flow meter. As the flow enters the quiescent plenum, three flow conditioning screens are used to ensure uniformity at the inlet of the film cooling holes. Inside the plenum, several thermocouples and pressure taps measure the coolant temperature and plenum pressure. The coolant temperature is about 250 K, and the mainstream temperature is about 300 K, which provides a density ratio of DR=1.2.

In order to approximate an adiabatic endwall condition, film cooling holes are machined from low conductivity Dow Styrofoam (k = 0.029 W/m-K). In each tested case, five holes are machined in the Styrofoam, each having a diameter of D=6.78 mm, a spanwise spacing of P/D=6, and an inclination angle of 30°. The 7-7-7 baseline hole used in this study was developed by Schroeder and Thole [1], and is shown in Figure 1. That hole was modified with larger expansion angles to create the 12-12-12 hole. The area ratio was modified by increasing the length of the diffuser, L_{diff}, while maintaining expansion angles. The modified hole designs for the cases examined in this study are shown in Figure 3, where the nomenclature for the cases indicates the area ratio (e.g., AR2 has an area ratio of 2 between the outlet plane of the hole to the meter).

A FLIR T650sc infrared camera was used to capture the surface temperature of the adiabatic Styrofoam endwall. An in-situ calibration using surface copper block thermocouples was done in order to ensure the accuracy of the camera calibration for the range of temperatures tested. Adiabatic effectiveness measurements made by Eberly and Thole [20] for cylindrical holes in this facility showed good agreement with the literature.

Flowfield measurements for this study were taken using a high-speed particle image velocimetry (PIV) system. The PIV system includes a dual-head Nd:YLF laser and two high speed cameras in a stereo configuration, shown in Figure 4. The laser is capable of 20 mJ per pulse per head at a 1 kHz repetition rate with 170 ns pulse width. The cameras have 1280x1024 pixel resolution with a 105 mm lens and a capture frequency of 2,000 frames per second at full resolution. The system was controlled by LaVision software and the calculation was done using DaVis 8. For this study, the optimal time step between image pairs was 30 μs, and the flowfield sampling rate was 500 Hz.

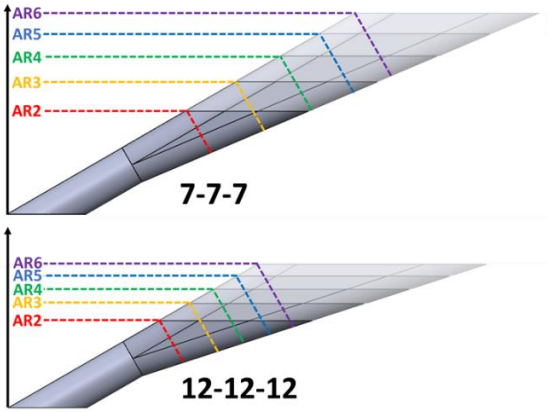

Figure 3. Range of area ratios for the 7-7-7 and 12-12-12 holes.

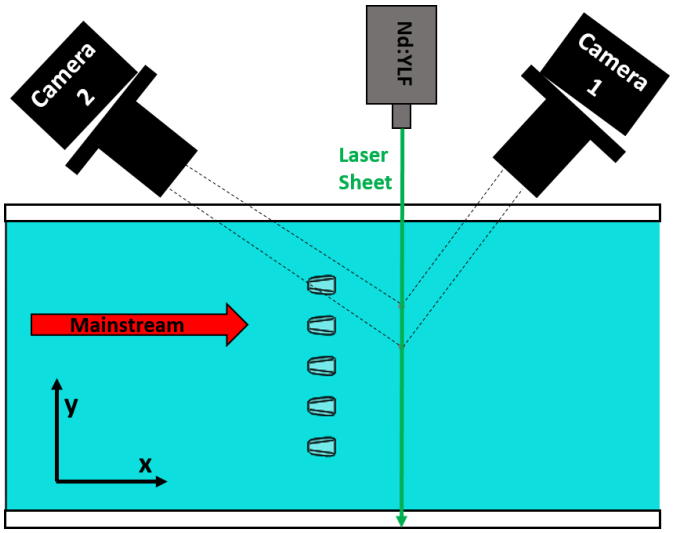

Figure 4. PIV setup for measurements at an x/D=10 crossplane.

The flowfield seeding particles used in these measurements was di-ethyl-hexyl-sebecat (DEHS), which was fed into the coolant loop of the tunnel via an aerosol generator which provided a mean particle diameter of 1 μm. The Stokes number based on this diameter, and based on a flow timescale of D/U_c=0.1 m/s for M=6.0, was 0.03, which is well below unity and thus indicates that the seed follows the flow. The tunnel is recirculating, so even though seed was only added in the coolant loop, the mainstream flow also had an appropriate particle density after a short period.

UNCERTAINTY ANALYSIS

Using the propagation of measurement uncertainties analysis outlined by Figliola and Beasley [21], the experimental uncertainty was found for blowing ratio, density ratio, adiabatic effectiveness, and PIV flowfield measurements. All calculations were done using a confidence interval of 95%.

Uncertainty in blowing ratio was found to be ±5% for all blowing ratios, which is mostly due to the bias uncertainty in the mainstream Pitot probe pressure transducer and also the coolant Venturi flowmeter (±0.25% of full-scale flow and verified by separate tests with a laminar flow element in series). For density ratio, the uncertainty was less than ±0.01 for all cases. The total uncertainty in adiabatic effectiveness was estimated to be $\delta\eta$ = ±0.034, which is largely due to a high bias uncertainty of $\delta\eta_b$ = ±0.027, which would be the same for each test. This bias uncertainty for effectiveness is based on a surface temperature uncertainty of ±1.31 ºC, which is caused by scatter in the in situ infrared camera calibration and also the bias uncertainty of the thermocouples.

Repeatability was confirmed by retesting a case, including a case that had been removed and reinstalled. The maximum difference in area-averaged effectiveness was 0.012, and the maximum difference in laterally-averaged effectiveness was 0.015. Periodicity was also very good for all cases, which is determined visually and quantitatively for the three holes over which the experimental results are averaged, as shown in Figure 5. For both AR2 and AR6 at M=3.0, there is good agreement qualitatively in the contours of Holes 2, 3, and 4, and also in the laterally averaged effectiveness for all three. Only one hole's contours is shown in the ensuing figures, but all holes have similarly good periodicity, so it is representative of all holes.

Uncertainty in the PIV measurements was calculated for a previous study in this facility with the same setup [22], and the uncertainty in the through-plane velocity component was found to be ±4.8%, and the in-plane uncertainty was a maximum of ±8%. These uncertainties were based on a conservative estimate of ±0.15 pixel instantaneous displacement uncertainty. A case was repeated for a slightly larger time step of 40 μs, and the time-averaged results agreed within the above reported uncertainty. Also, statistical convergence of time-averaged images was found by averaging over 1000, 1500, and 2000 images, all with good agreement in the average velocity.

COMPUTATIONAL SETUP

The mesh used for the CFD cases was created using Pointwise, and was made using a method and cell size previously determined to be grid independent and to have $y^+<1$ on all walls by Haydt et al. [19]. This domain is shown in Figure 6 with labeled boundary conditions. The inlet velocity profile was calculated using TEXSTAN based on a known approach length and matched to a measured boundary layer upstream of the holes.

ANSYS Fluent was used to solve the conservation equations, using the realizable k-ε turbulence model. The cases were run for 1000 iterations with first order discretization, and then for 3000-5000 iterations with second order discretization. Convergence was ensured through laterally-averaged η monitors on the surface, and point temperature monitors slightly above the endwall, in a manner similar to Haydt et al. [19].

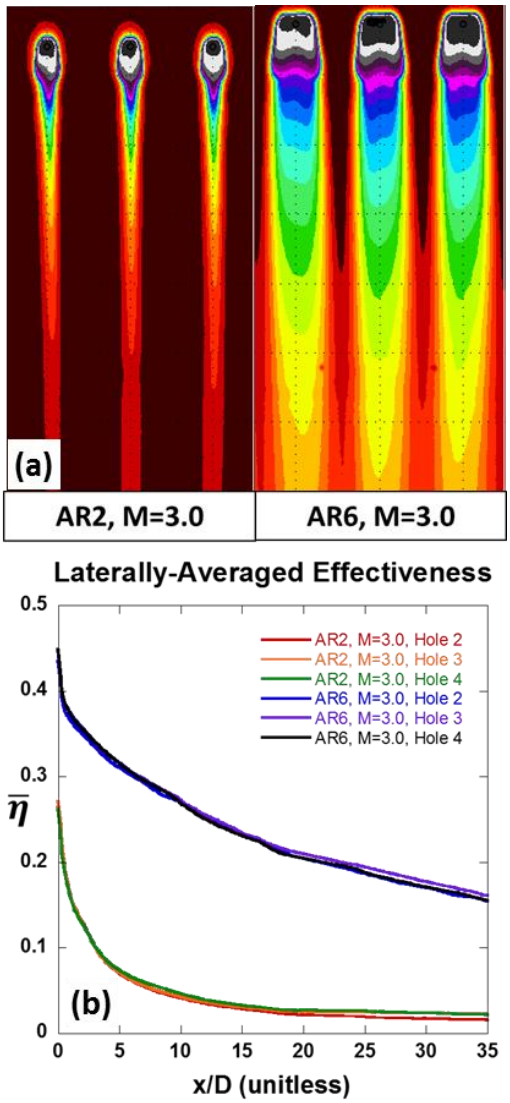

Figure 5: 7-7-7 AR2 and AR6 holes both at M=3.0, showing periodicity within experimental uncertainty in the adiabatic effectiveness contours (a) and in the laterally averaged effectiveness plot (b).

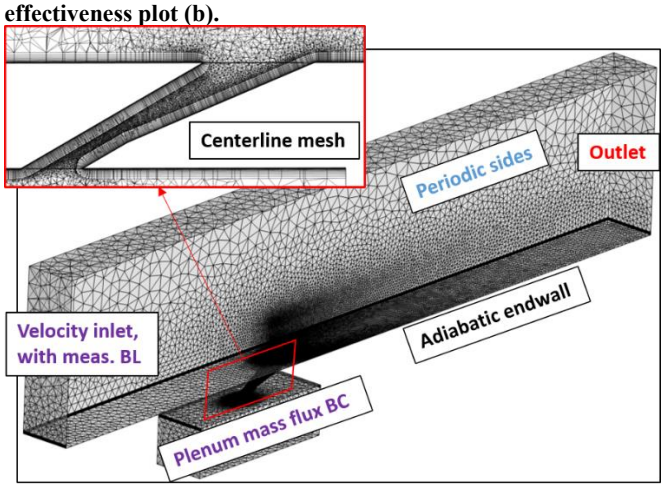

Figure 6. CFD domain with boundary conditions and a depiction of the centerline mesh resolution.

DISCUSSION OF RESULTS

First, for film cooling holes with a pre-determined blowing ratio, the effect of area ratio is shown. Next, for holes with a pre-determined area ratio, the effect of blowing ratio is shown. For holes with a limited wall thickness, the effect of expansion angle is discussed. Next, the results are discussed in concert to determine an optimal design point for large area ratio film cooling holes. Finally, the adiabatic effectiveness measurements are explained via CFD predictions and PIV measurements.

Effect of Area Ratio

A desired location for a film cooling hole on an airfoil might have a pre-determined pressure difference between the internal and external flow, and thus an estimated blowing ratio range. In this section, the effect of area ratio on a moderate, high, and very high blowing ratio is discussed.

Figure 7 shows measured adiabatic effectiveness contours for a moderate blowing ratio of M=1.0, for all tested area ratios of the 7-7-7 hole. Since the blowing ratio is determined based on the metering section area, all of these cases have an identical average velocity at the metering section. However, due to the relative diffuser sizes, the average velocities at the exit areas are much different. As the area ratio and diffuser footprint width get larger the contours widen, but the effectiveness level at the trailing edge of the hole decreases. This could be explained by mainstream ingestion and over-diffusion occurring in the diffusers of the large area ratio holes. As a result, the coolant exiting from the trailing edge of the holes with larger diffusers has a higher temperature than exists in the coolant plenum.

Despite the lower levels of effectiveness immediately at the trailing edge for the higher area ratio holes, the larger breakout width of those diffusers provides a wider swath of coolant on the endwall, especially just downstream of the holes. Laterally-averaged effectiveness curves in Figure 8 show that this larger coverage mostly offsets the detrimental mixing that occurs in the large diffusers, since the larger area ratio holes have higher laterally averaged effectiveness immediately downstream of the trailing edge.

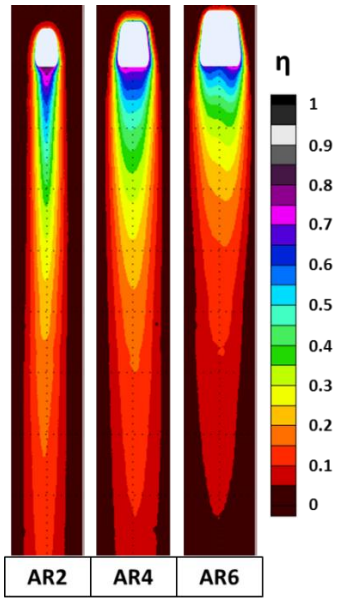

Figure 7. Contours of measured adiabatic effectiveness for all 7-7-7 area ratios, all at M=1.0.

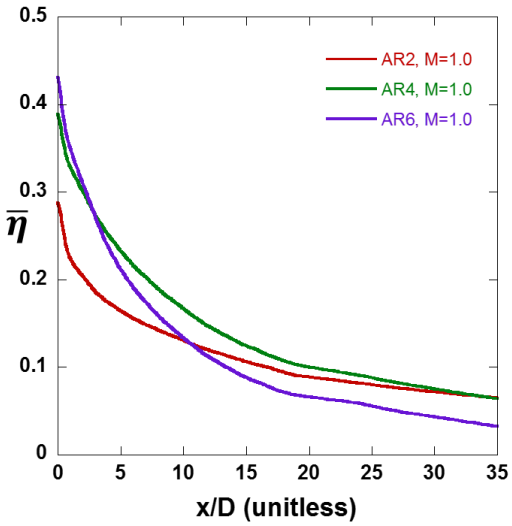

Figure 8. Laterally-averaged effectiveness for all 7-7-7 area ratios, all at M=1.0.

At a higher blowing ratio of M=3.0, different patterns emerge in the measured effectiveness contours, shown in Figure 9. In film cooling literature, M=3.0 is often one of the higher blowing ratios considered, since holes with more typical area ratios between 2 and 3 generally start to see decreased performance before this point [2] due to jet detachment. The narrowing of the effectiveness contours in Figure 9 for low area ratios (as compared to Figure 7) for this blowing ratio appear to support the trend of jet detachment above M=3.0 which is observed in the literature. The narrowing contour indicates the jet is penetrating further into the mainstream. However, this is not the case for the larger area ratio holes. These contours are wider than their lower blowing ratio counterparts from Figure 7, and the effectiveness levels extend much farther downstream. Also, the effectiveness levels immediately at the trailing edge for the larger area ratio holes are much higher than they were for the M=1.0 case, and they are only slightly lower than that of the lower area ratio cases. This suggests that less mainstream ingestion is occurring at the higher blowing ratios.

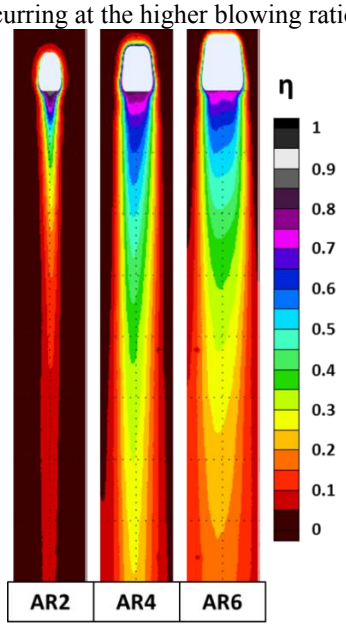

Figure 9. Contours of measured adiabatic effectiveness for all 7-7-7 area ratios, all at M=3.0.

At the highest blowing ratio of M=6.0, it is clear from the adiabatic effectiveness contours in Figure 10 that a low area ratio is a disadvantage at this blowing ratio. The contours for AR2 and AR4 have both narrowed compared to Figure 9, while the contours of AR6 remain wide, and have contour levels extend even further downstream. Also, the effectiveness level right at the trailing edge of the AR6 hole is about the same for each case, which suggests that over-diffusion and mainstream ingestion is likely not occurring in the larger diffuser holes at this very high blowing ratio.

The laterally-averaged effectiveness curves of Figure 11 also confirm that the large area ratio holes have a clear advantage at this blowing ratio, since the effectiveness increases as area ratio increases. Also, there is a much larger spread in performance between the high blowing ratio case of Figure 11 and the low blowing ratio case of Figure 8.

Effect of Blowing Ratio

For holes with a pre-determined area ratio, it would be helpful for designers to know how that type of hole will respond to a wide range of blowing ratios. This section examines the 7-7-7 at three area ratios and shows the effect that blowing ratio has on their adiabatic effectiveness.

The smallest area ratio tested, the 7-7-7 AR2, was experimentally run at blowing ratios ranging from a moderate M=1.0, to a high M=4.0, to a very high M=6.0. The adiabatic effectiveness contours for these cases are shown in Figure 12.

For this small area ratio, high blowing ratios result in increased mainstream penetration and poor effectiveness, which is consistent with what was observed by Schroeder [1] for a similarly shaped hole. Jet liftoff appears to occur by M=3.0, beyond which there is very little change in the contours.

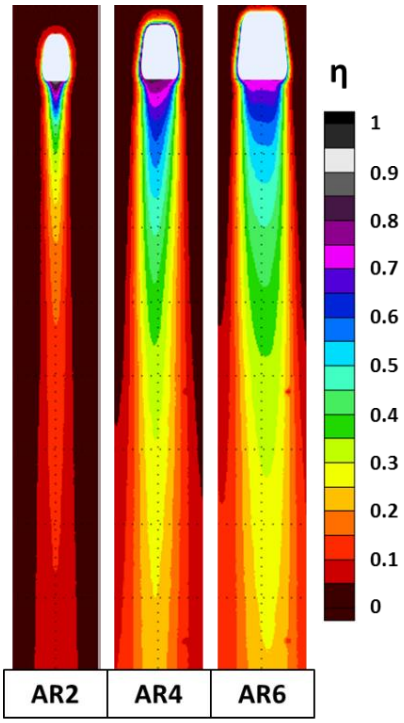

Figure 10. Contours of measured adiabatic effectiveness for all 7-7-7 area ratios, all at M=6.0.

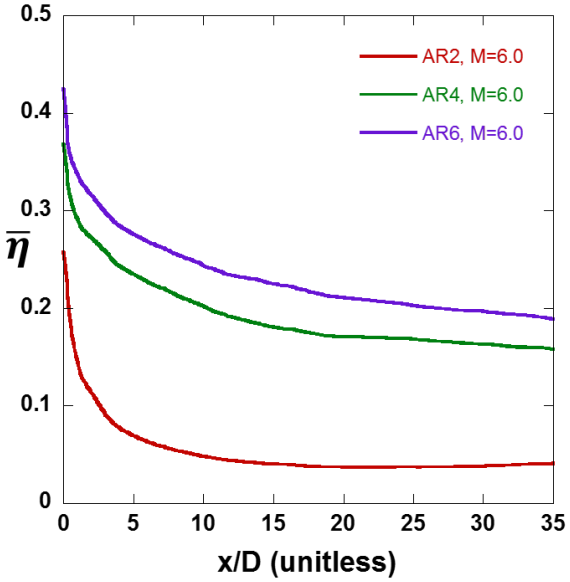

Figure 11. Laterally-averaged effectiveness for all 7-7-7 area ratios, all at M=6.0.

When the area ratio is doubled to AR=4, high effectiveness is observed for high blowing ratios, since the longer diffuser can reduce the jet velocity more significantly. This can be seen from the adiabatic effectiveness contours in Figure 13. The contours indicate the performance of the AR4 hole peaks around M=3.0, then decreases slightly for very high blowing ratios. Therefore, for the AR4 hole, the effectiveness increases up to an optimal blowing ratio, but any additional coolant beyond that results in diminished or decreased returns.

The largest area ratio case, 7-7-7 AR6, appears to constantly increase in cooling performance up to very high blowing ratios, as indicated by the contours in Figure 14 and the laterally-averaged effectiveness curves in Figure 15.

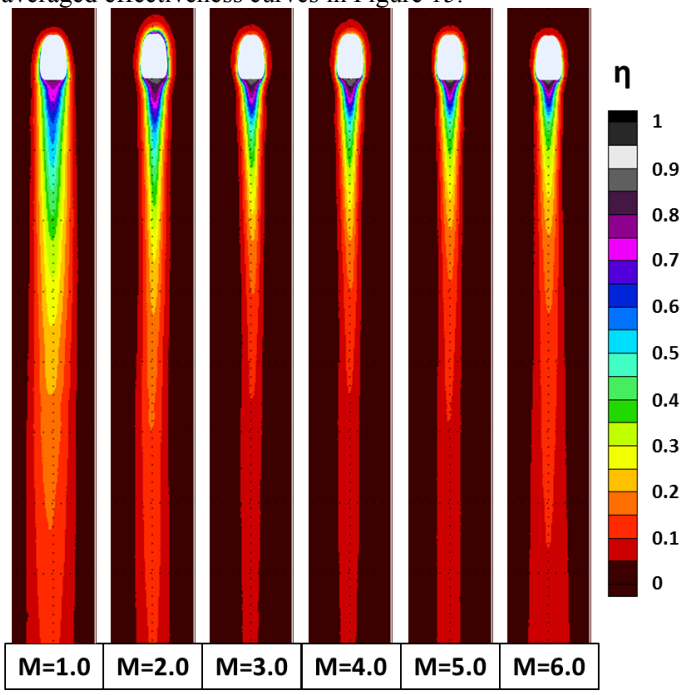

Figure 12. Contours of measured adiabatic effectiveness for the 7-7-7 AR2 case at all blowing ratios.

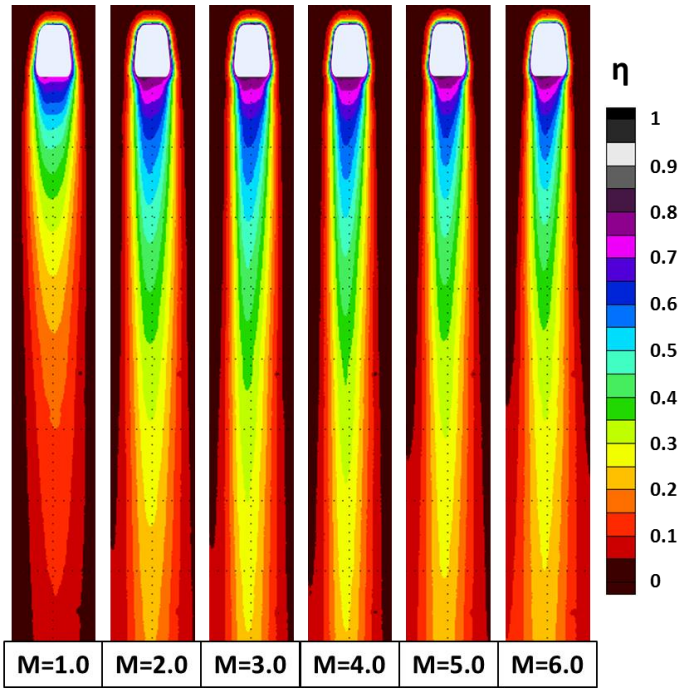

Figure 13. Contours of measured adiabatic effectiveness for the 7-7-7 AR4 case at all blowing ratios.

For the AR6 case, the contours are all very wide due to the breakout width of the diffuser. As the blowing ratio increases, the levels of high effectiveness extend farther downstream, which indicates more coolant near the wall. This is obviously advantageous to film cooling effectiveness, as is shown by Figure 15. Laterally-averaged effectiveness plateaus at the highest blowing ratios, and any additional coolant beyond that point does not appear that it would significantly increase the effectiveness.

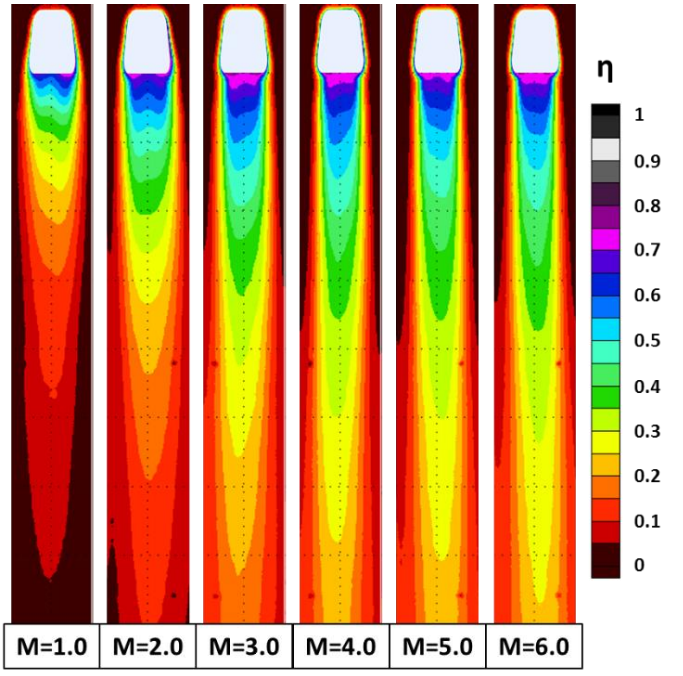

Figure 14. Contours of measured adiabatic effectiveness for the 7-7-7 AR6 case at all blowing ratios.

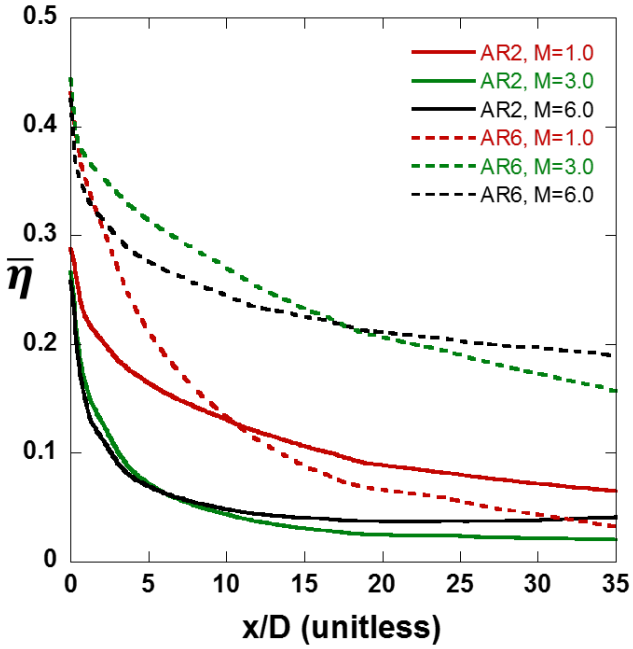

Figure 15. Laterally-averaged effectiveness for the largest and smallest area ratio at a range of blowing ratios.

Effect of Expansion Angle

For film cooling holes in which there is a pre-determined wall thickness, a certain area ratio can be achieved via larger expansion angles. The following section compares a moderate and a large expansion angle at the same blowing ratios and area ratios. Since the area ratios are kept equal between the respective 7-7-7 and 12-12-12 holes, that means the area at the exit plane of the diffuser, A_{exit}, is equal. Since the expansion angles are different, however, a 12-12-12 hole will have a shorter L_{diff}/D and a larger breakout width than the 7-7-7.

Figure 16 shows measured adiabatic effectiveness contours for three area ratios, AR2, AR4, and AR6, of the 7-7-7 and the 12-12-12, all at a relatively high blowing ratio of M=3.0. For both hole types, it is clear that there is a trend of increasing effectiveness with increasing area ratio. The large holes however, despite their increased lateral coverage of coolant, have very low effectiveness levels immediately at the trailing edge of the hole. This is especially true for the 12-12-12 hole: Every area ratio case of the 12-12-12 has lower trailing edge effectiveness than its corresponding 7-7-7 case. Due to the larger expansion angles of the 12-12-12 hole, the size of the diffuser where it breaks out onto the surface is larger than the 7-7-7, even though the area ratio (defined in Figure 1) is equal. This means that the 12-12-12 hole is more susceptible to mainstream ingestion and in-hole mixing, which is borne out by the effectiveness contours.

The detrimental effect of over-diffusion and mainstream ingestion can be seen in the corresponding laterally-averaged effectiveness curves in Figure 17. Each 12-12-12 case has a slightly lower laterally-averaged effectiveness at x/D=0, with the smallest detriment at AR2, which would have the least amount of ingestion due to being the smallest diffuser. However, the penalties on effectiveness due to the mixing in the larger diffusers is offset by the larger lateral coverage of the 12-12-12 coolant jet, at least for the AR2 and AR6 case, relative to the 7-7-7 hole.

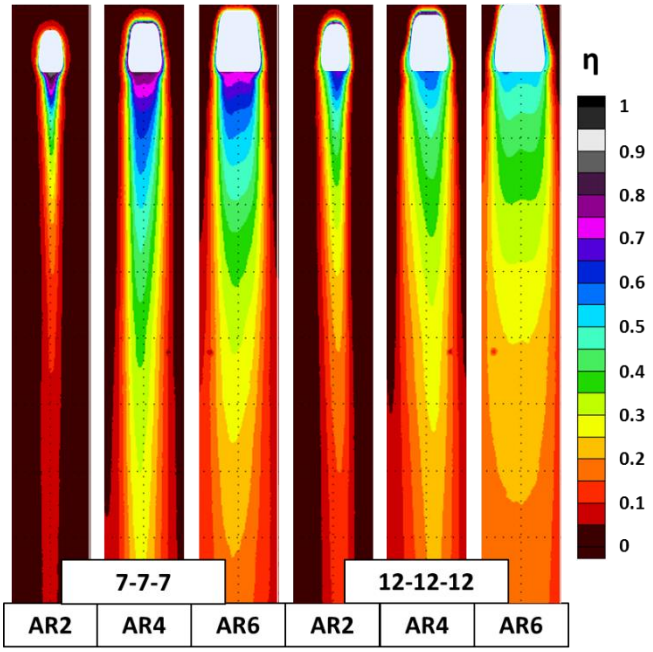

Figure 16. Adiabatic effectiveness comparison between AR2, AR4, and AR6 of the 7-7-7 (left) and 12-12-12 (right) holes, all at M=3.0.

Even at the highest blowing ratio of M=6.0, the large 12-12-12 diffusers still experience increased mixing-out of the coolant at the diffuser exit, as evidenced by the contours in Figure 18. However, due to the larger breakout width, the lateral coverage of the coolant is greater for the 12-12-12 hole than for the 7-7-7. On a laterally-averaged basis in Figure 19, it appears that the increased lateral coverage makes up for increased mixing that occurs in the larger 12-12-12 diffuser.

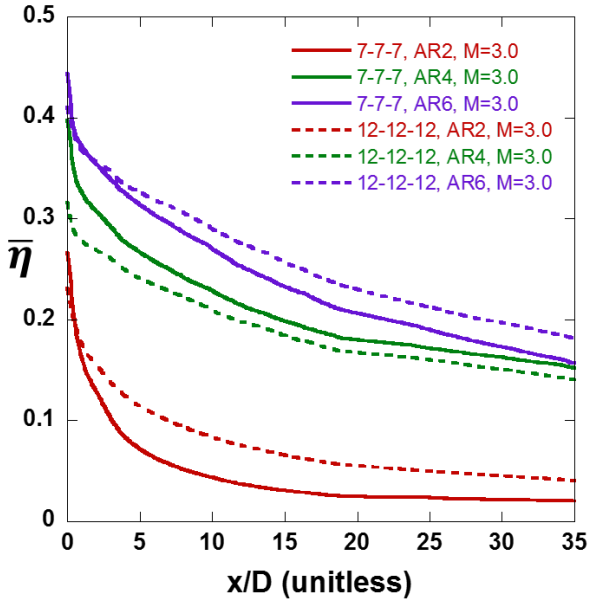

Figure 17. Laterally-averaged effectiveness for AR2, AR4, and AR6 of the 7-7-7 and 12-12-12 holes, all at M=3.0.

No unsteadiness was observed in the experimental measurements of the 12-12-12 hole, so the mixing that occurs in the diffuser of the larger 12-12-12 holes is probably not due to large scale unsteadiness associated with the jet separating from the diffuser sidewalls. From the data presented in this section, it appears that the expansion angle of the diffuser has just a small effect on the laterally-averaged effectiveness due to two competing trends: increased ingestion and mixing in a large diffuser, but increased lateral coverage of coolant.

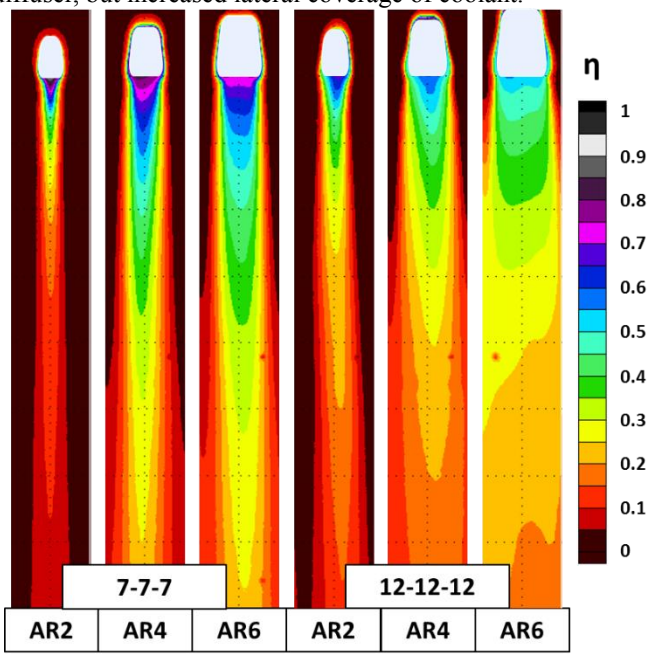

Figure 18. Adiabatic effectiveness comparison between AR2, AR4, and AR6 of the 7-7-7 (left) and 12-12-12 (right) holes, all at M=6.0.

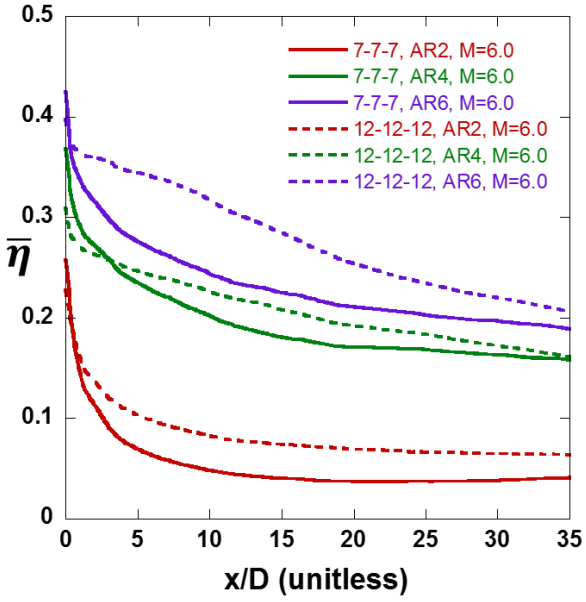

Figure 19. Laterally-averaged effectiveness for AR2, AR4, and AR6 of the 7-7-7 and 12-12-12 holes, all at M=6.0.

Optimal Area Ratio Design

From the data presented thus far, it seems that for a given area ratio, a hole has an optimal blowing ratio at which it gives its highest effectiveness, beyond which the effectiveness either plateaus or decreases. Figure 20 shows the area-averaged effectiveness for every case that was experimentally run versus the blowing ratio, in order to depict the optimal blowing ratio for the experimental cases. As the area ratio increases, the blowing ratio at which it experiences peak effectiveness also increases. Also, for any given blowing ratio, except perhaps the lowest

blowing ratio of M=1.0, the effectiveness increases with increasing area ratio.

The reason for the success of high area ratio holes which enable very high blowing ratios is two-fold:

First, the large area ratio enabled by a long diffuser with moderate expansion angles is effective at smoothly reducing high hole inlet velocities. For a shorter diffuser with equal area ratio and more extreme expansion angles, it is likely that sidewall separation would occur, and the film cooling performance would degrade, as shown by Kohli and Thole [10]. Maintaining the moderate expansion angle and increasing the diffuser length has allowed the film cooling hole to operate more similarly to a classical conical diffuser. The coolant velocities associated with the very high blowing ratios being tested would traditionally result in jet separation, but the large, long diffusers of these film cooling holes reduce that velocity while still maintaining the high mass flow rate of coolant to the endwall.

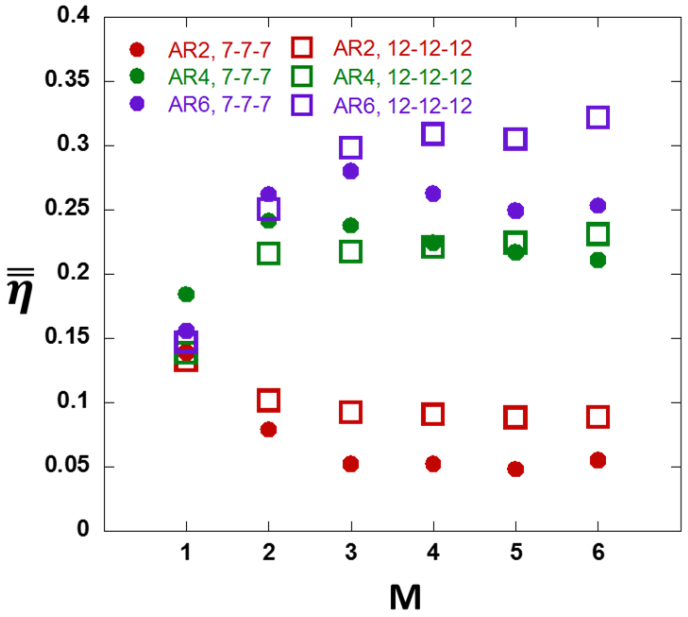

Figure 20. Area-averaged effectiveness for all experimental cases vs. blowing ratio. 7-7-7 with solid symbols, 12-12-12 with open symbols.

Second, the large diffusers have very large breakout widths on the endwall surface, which significantly increases the lateral spread of coolant. As the area ratios increase and the diffusers get larger, the breakout width takes up an increasing percentage of the span of the film cooling hole, approaching that of an ideal film cooling slot. This is especially true for the 12-12-12 hole.

Both of these advantageous effects can be accounted for by normalizing the data of Figure 20. First, the blowing ratio is normalized by the area ratio in order to created an "effective blowing ratio", M/AR. Since the blowing ratio is defined by the metering section area, the average velocity in the metering section is identical between cases of like blowing ratio. However, due to the diffusion of the coolant, the average velocity at the exit plane of the hole is reduced, and can be approximated as reduced by a factor of the area ratio. Next, the area-averaged effectiveness is normalized by the percentage of the span that the breakout width takes up, or t/P. This accounts for the advantageous lateral spread of coolant by the holes with larger diffusers, and gives an idea of the kind of cooling a hole can provide on a "per unit wall" basis. This normalized experimental data is shown in Figure 21.

On these nomalized axes, the 7-7-7 experimental data appear as curves with a common peak around M/AR=0.5. The data for the 12-12-12 hole does not collapse as well to this same peak, but this might be because of the increased in-hole mixing that occurred for the large diffusers of the 12-12-12 hole.

The peak in the 7-7-7 data suggests that this is the optimal effective blowing ratio for the 7-7-7 hole. Designers can use this curve in order to find the optimal combination of blowing ratio and area ratio in order to get maximum effectiveness for a film cooling application. If the blowing ratio is pre-determined, an area ratio should be picked which will bring the effective blowing ratio at the exit plane down to around M/AR=0.5. However, as was previously stated, for the range of area ratios tested, increasing the area ratio always increased the effectiveness for any given blowing ratio except M=1.0. Alternately, if the area ratio is set, this curve can be used to find the optimal blowing ratio that will provide peak effectiveness or a point beyond which extra coolant will bring diminishing returns.

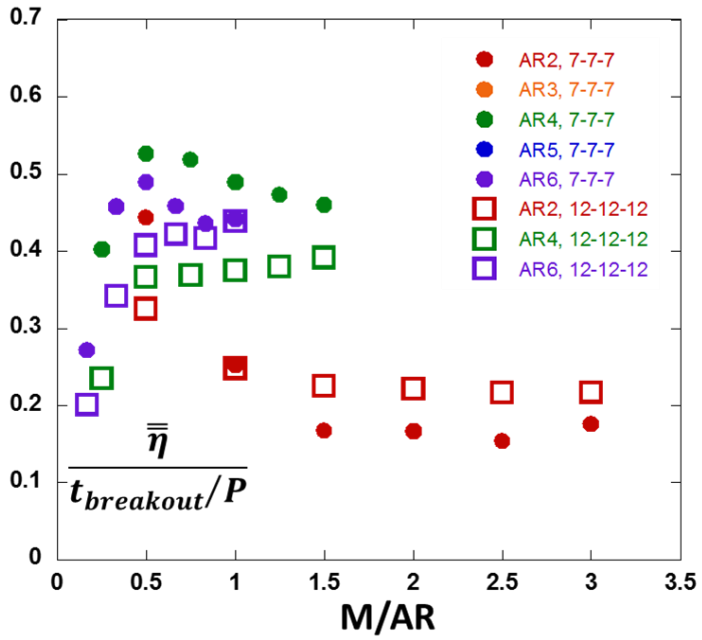

Figure 21. Area-averaged effectiveness normalized by breakout width versus effective blowing ratio.

Figure 22 shows data from Gritsch et al. [7] that is normalized in the same way, and based on this plot, it appears that this data from literature also has a peak normalized area-averaged effectiveness at around the same effective blowing ratio. In that study, blowing ratios as high as the ones in the current study were not tested, so the curve does not continue on to higher values of M/AR, but it does appear that beyond the same optimal M/AR for the 7-7-7 hole, the Gritsch et al. data begins to drop off in normalized performance.

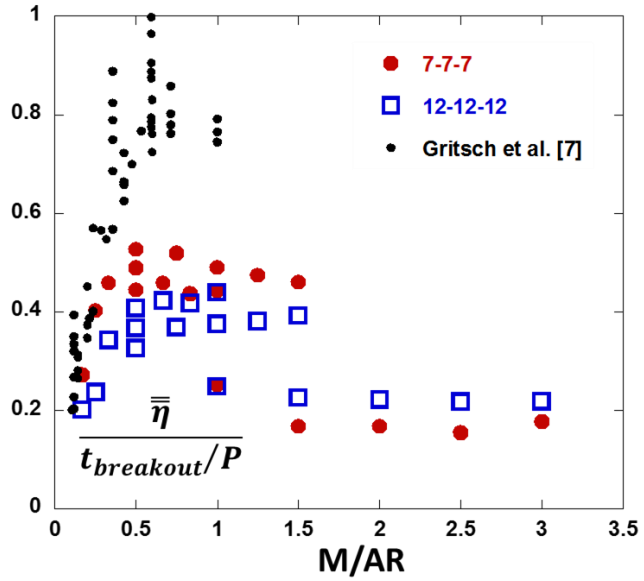

Figure 22. Area-averaged effectiveness normalized by breakout width versus M/AR, including data from Gritsch et al. [7].

Computational Predictions

A CFD simulation was run for each experimental case, and even though the exact values of area-averaged effectiveness were not correctly predicted, the CFD did predict the trend of increasing effectiveness with increasing area ratio. There were several key elements of the experimental results that the CFD did not match, and that is made clear by comparing the adiabatic effectiveness contours in Figure 23.

Based on these contours, it appears that there are several important differences between the CFD and the experiments. First, the effectiveness levels at the trailing edge for the CFD predictions are much higher than they actually are experimentally. This suggests that the CFD is not properly capturing the mixing and over-diffusion that is occuring in these large diffusers. Additionally, the CFD cases are run with an adiabatic surface material, whereas in the experiment it is only an approximation. So it is possible that some conduction losses are occuring in the hole experimentally, which is not accounted for by the CFD, and could also explain the lower trailing edge effectiveness. Second, the CFD contours are not as wide as the experimental cases, suggesting that the CFD is underpredicting the lateral diffusion of the coolant jet. Finally, the CFD is predicting that effectiveness levels extend much further downstream than they do experimentally, which shows that the CFD is underpredicting the mixing that occurs between the coolant jet and the mainstream flow. These mispredicitons are well-known, and consistent with previous comparisons made for this facility and for the 7-7-7 hole in particular [19].

All of these underpredicted factors by the CFD result in local, laterally-averaged, and area-averaged effectiveness values that do not match the experimental results. However, the CFD was able to capture the important trends of this data, which can be seen from Figure 24. The CFD correctly predicts that as the area ratio increases, for a given blowing ratio, the effectiveness also increases. Also, the CFD predicted that each specific area ratio has an optimal blowing ratio at which it gets maximum cooling performance, and that this optimal blowing ratio increaes as area ratio increases. It did not, however, predict the correct optimal blowing ratio for each area ratio case. Also, the CFD predicts that the 12-12-12 significantly outperforms the 7-7-7, especially at low area ratios, which is not consistent with the experimental results from Figure 20. This can be explained by the poor capability to predict over-diffusion, which may be large factor in the performance of the 12-12-12 hole.

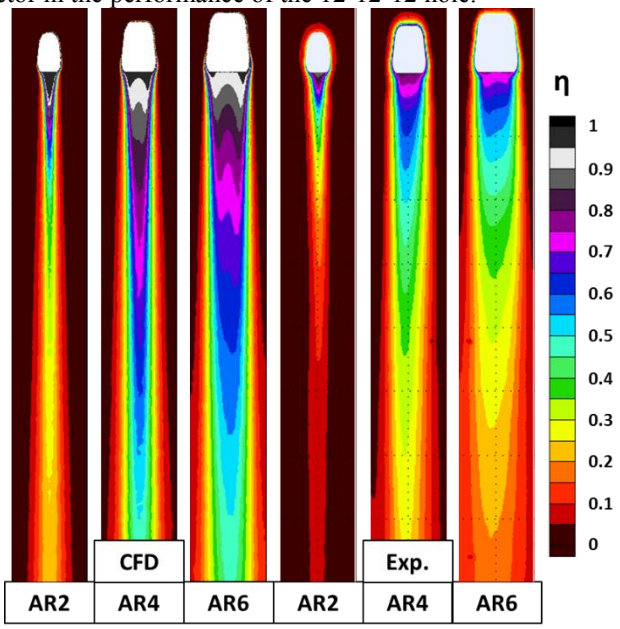

Figure 23. Predicted and measured adiabatic effectiveness contours for AR2, AR4, and AR6 of the 7-7-7 hole, all at M=3.0.

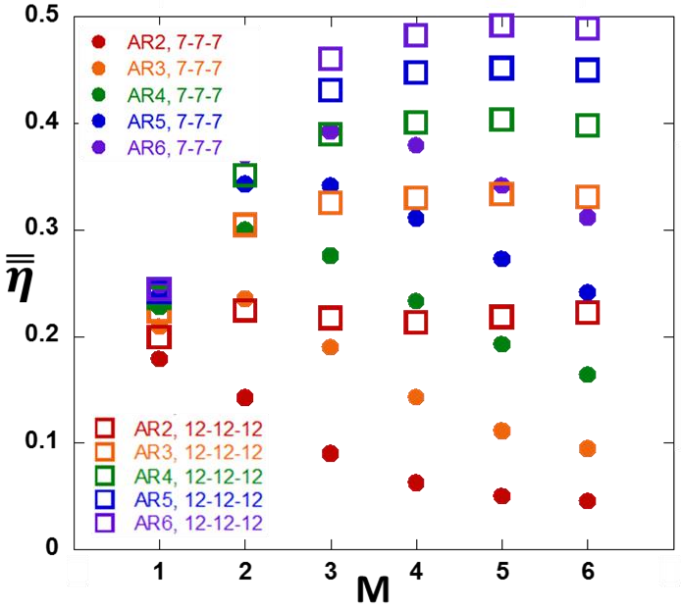

Figure 24. Area-averaged effectiveness for the simulations of all area ratio cases of the 7-7-7 and 12-12-12 holes.

As previously mentioned, these two holes have an identical mathematical exit area at each respective area ratio, and therefore the same "effective blowing ratio", but the shapes of the diffusers are different beyond that exit plane due to the changed expansion angles. Decreasing the effective blowing ratio of a hole also decreases its mainstream penetration, which is advantageous to effectiveness, due to the reduction in the upwards component of velocity. The 12-12-12 hole takes this a

step further by also reducing the ejection angle of the coolant jet, due to the larger forward expansion angle. The reduction in the ejection angle provides an additional decrease to the upwards velocity component, and therefore keeps the coolant jet closer to the endwall as compared to the 7-7-7 hole at the same blowing ratio and area ratio.

This reduced ejection angle and its ensuing effect on the film cooling effectiveness can be seen in Figure 25. Shown in this figure are centerline planes contoured by ϕ for the AR2 case at M=6.0. At this area ratio, even though the average velocity at the exit plane is roughly equal, the 12-12-12 has less mainstream jet penetration than the 7-7-7, which enables the coolant to remain close to the wall and spread laterally across the span.

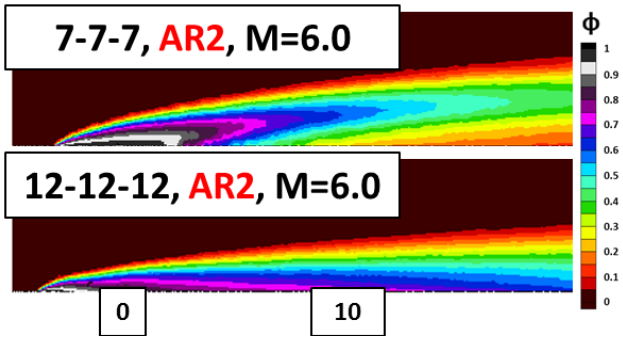

Figure 25. Predictions of centerline planes contoured by nondimensional temperature, for AR2 cases at M=6.0.

The lowered ejection angle is presumably an advantage that the 12-12-12 has experimentally as well, but that advantageous effect is effectively negated by the overdiffusion in those holes, which the CFD does not seem to predict. The jet is likely remaining attached to the wall in the experiments, but so much mixing has occurred in the diffuser that even if the coolant is covering the entire span, it is doing so at very low effectiveness levels.

Since the lowered ejection angle of the 12-12-12 is a secondary mechanism to keep the jet attached, it is reasonable to assume that the optimal effective blowing ratio will be different for the 12-12-12 and 7-7-7 holes, as predicted by CFD. This is clear from Figure 26, which plots the area-averaged effectiveness normalized by breakout width versus the effective blowing ratio. The CFD does predict a similar optimal effective blowing ratio for the 7-7-7 as was found from the experimental results, which is M/AR=0.5-0.75. The 12-12-12 predictions do not collapse to a curve, which the experimental data did not do either.

To understand why an effective blowing ratio of about 0.6 is optimal for the 7-7-7 hole, two cases were examined more closely: AR4 at M=2.0, which has an optimal M/AR=0.5, and AR4 at M=6.0, with a non-optimal M/AR=1.5. The exit planes for these two cases are shown in Figure 27 contoured by the jet velocity normal to the exit plane normalized by the mainstream velocity. In each case, there is a high velocity region near the top of the exit plane. Due to its position, this high velocity core region will be the first part of the jet to interact with the mainstream flow, creating a shear layer that will in turn form the counter rotating vortex pair (CRVP). In the high blowing ratio case, there is a large difference between the jet velocity and the mainstream velocity, so a strong shear layer will be formed. Alternately, in the M/AR=0.5 case, the high velocity core of the coolant jet has roughly the same velocity magnitude as the mainstream flow, and thus a weak shear layer will be formed, and therefore a weaker CRVP. A strong CRVP lifts the coolant jet up and away from the surface and is detrimental to film cooling performance. Since the data in Figure 26 is normalized by breakout width, the primary driver for relative performance on this curve is coolant jet attachment. Film cooling holes with M/AR=0.5 maintain jet attachment due in part to the weak CRVP formed by an ideal match between the coolant jet and mainstream velocity.

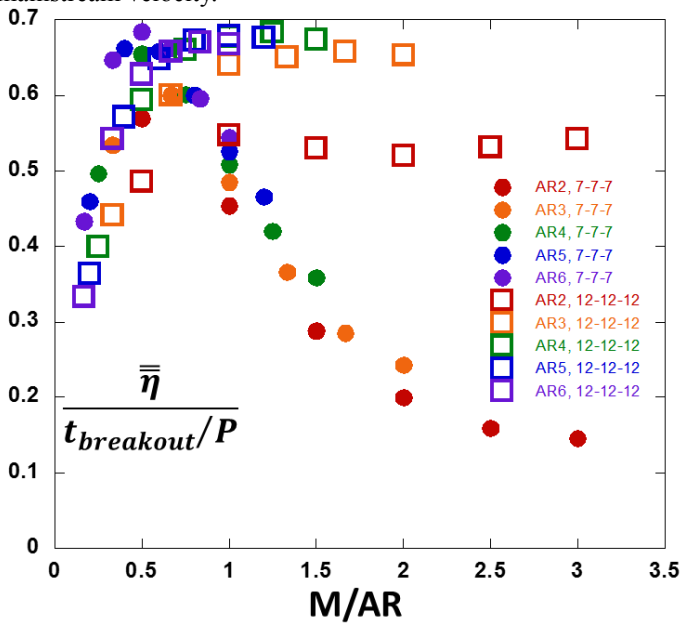

Figure 26. Normalized area-averaged effectiveness plotted versus effective blowing ratio for all simulated cases of the 7-7-7 and 12-12-12 holes.

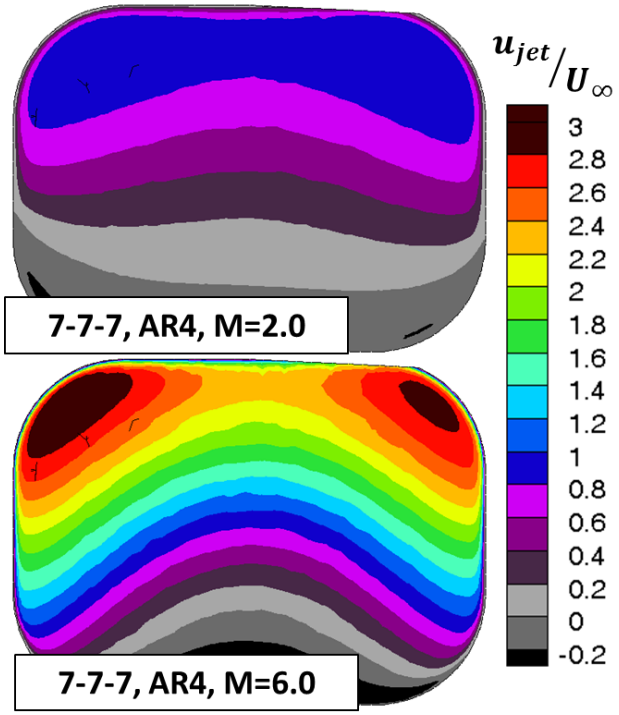

Figure 27. Predicted contours of jet velocity at the exit plane for a case at the optimal effective blowing ratio of M/AR=0.5, and the same area ratio at a higher blowing ratio.

Conical Diffuser Comparison

As previously mentioned, the high velocity regions in the exit area are due to the non-uniform velocity profile in the metering section caused by jetting. These high velocity regions are impactful on the performance of the cooling hole, but in a broader sense, the reduced average velocity in the exit plane is also a factor in these large area ratio holes' high performance, and that is a result of the shaped hole diffuser.

A conical diffuser has a theoretical ideal pressure recovery, which is defined as $1-(1/AR)^2$. The efficiency of the diffuser is the ratio of the actual pressure recovery coefficient to the ideal one. The pressure recovery coefficient is defined as follows:

$$c_p = \frac{(P_{exit} - P_{inlet})}{\frac{1}{2}\rho {U_{inlet}}^2}$$

A similar analysis of pressure recovery was performed in this study, using the computational predictions. The pressures here are defined as the area-weighted average static pressure at the exit plane and diffuser inlet plane, and the velocity is the area-weighted average velocity magnitude at the diffuser inlet.

Of course, the comparison to a conical diffuser is not a perfect comparison since there are two important differences. First of all, the diffuser of the 7-7-7 and 12-12-12 holes is not conical, but rather a loft from a circle to a square with rounded edges. Second, for many conical diffuser studies, it is assumed that the inlet and exit conditions are uniform, whereas in the case of film cooling the inlet condition is non-uniform and the exit condition is into crossflow.

Figure 28 shows the predicted diffuser efficiency for the 7-7-7 and 12-12-12 simulations for all blowing ratios and area ratios. The 7-7-7 hole has a much more efficient diffuser than the 12-12-12 at all blowing ratios. This means that the 7-7-7 is better able to stagnate the inlet velocity and convert it into static pressure at the exit plane. Cases with higher diffuser efficiencies and thus higher static pressure at the exit plane correlate to cases with less mainstream ingestion, as seen in the experimental contours. This suggests that a hole with a lower diffuser efficiency, such as the 12-12-12 hole, are more susceptible to unsteadiness and separation in the diffuser, and mainstream ingestion that could lower the centerline effectiveness.

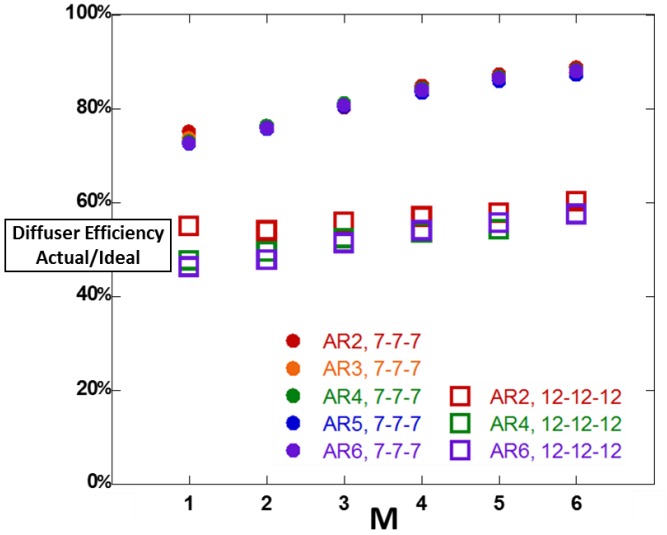

Figure 28. Diffuser efficiency plotted versus blowing ratio for all simulated cases.

Particle Image Velocimetry Flowfield Data

Particle Image Velocimetry (PIV) data was collected for three blowing ratios (M=1.0, M=3.0, and M=6.0) for the lowest and highest area ratios, AR2 and AR6, all at a downstream plane normal to the mainstream flow direction located at x/D=10. Figure 29 (a) shows contours of the streamwise velocity component overlaid with vectors of in-plane velocity for the low blowing ratio of M=1.0 and AR2. Figure 29 (b) shows the same vectors and contours, with a different scale, for the highest blowing ratio of M=6.0, also at AR2. These two figures show the primary differences in the flowfield between the low and high blowing ratio cases. At the lowest blowing ratio, the velocity deficit due to the low velocity coolant jet is seen in the middle of the plane near the wall. Alternately, in the high blowing ratio case, the core has a much higher velocity than the mainstream flow, and has separated significantly from the wall.

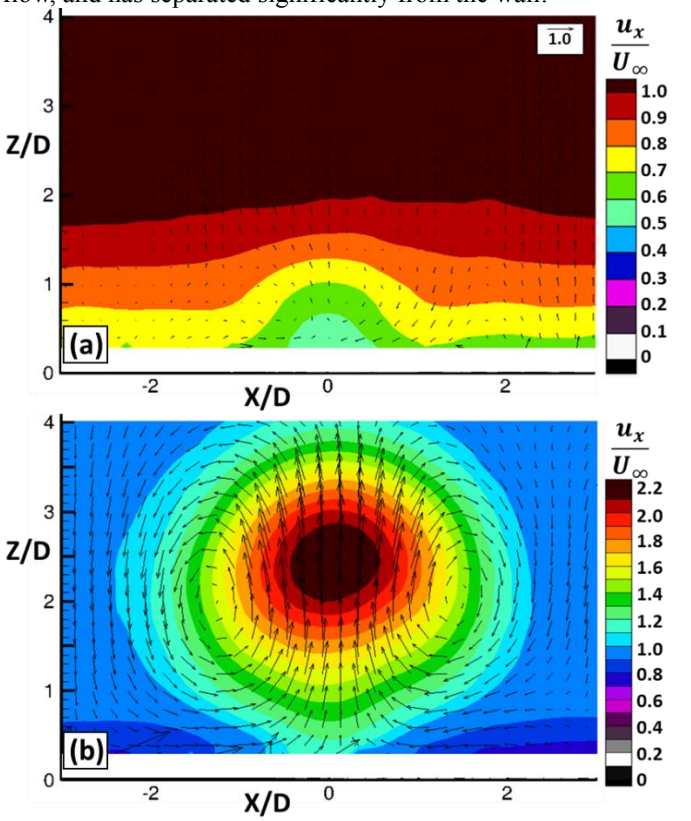

Figure 29. Downstream plane at x/D=10, contoured with x-velocity and overlaid with in-plane vectors, for the AR2 hole at (a) M=1.0 and (b) M=6.0.

The in-plane velocity vectors of these two cases also indicate the strength and size of the counter-rotating vortex pair (CRVP). For the low blowing ratio case, the in-plane velocity components are so small that the CRVP is not evident from the vectors. Alternately, in the high blowing ratio case, the CRVP is very large and dominates the extent of the measured flowfield.

The flowfield for the AR6 hole is very different from that of the AR2 hole, due to the large difference in jet velocity leaving the diffuser. Due to the increased diffusion in the AR6 holes, and the ensuing low-velocity coolant jets, the in-plane velocity components are very small, and do not indicate strong coherent vortices in either case. Figure 30 (a) shows the plane at x/D=10 contoured by normalized x-velocity and overlaid with in-plane velocity vectors for the AR6 hole at M=1.0, and Figure 30 (b)

shows the same for M=6.0, with a different contour scale. Similar to the AR2 low blowing ratio case, there is a velocity deficit due to the low-velocity coolant jet of the M=1.0, AR6 case, which remains close to the wall and spreads over most of the span. Alternately, the M=6.0 case has a jet core with a velocity slightly higher than the freestream velocity that is indicating slight mainstream penetration, despite the increased diffusion of the AR6 hole. This jet core has much lower velocity than the corresponding high blowing ratio case for the AR2 hole, shown in Figure 29a.

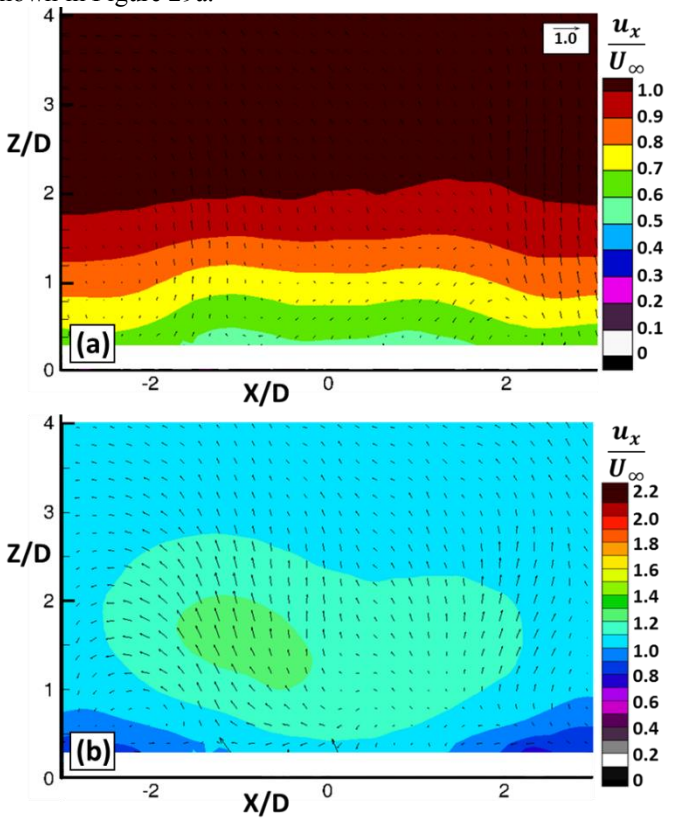

Figure 30. Downstream plane at x/D=10, contoured with x-velocity and overlaid with in-plane vectors, for the AR6 hole at (a) M=1.0 and (b) M=6.0.

CONCLUSIONS

Two shaped film cooling holes with different expansion angles were tested and simulated at a variety of area ratios and blowing ratios. The varying area ratios were created via extending the diffuser L/D while maintaining the diffuser expansion angles. Adiabatic effectiveness and particle image velocimetry measurements were collected, in addition to the cases being simulated in ANSYS Fluent using the realizable k-ε model.

Simulations predicted, and experiments confirmed, that adiabatic effectiveness increases with increasing area ratio for each blowing ratio that was investigated, and this is true for both the 7-7-7 and 12-12-12 holes. Additionally, for a given area ratio, there exists an optimal blowing ratio, an increase beyond which results in either a decline or plateau in cooling effectiveness. It was found that for the 7-7-7 hole, both experimentally and computationally, all cases have a common peak in optimal effective blowing ratio, M/AR of approximately 0.6. Further investigation via CFD yielded the conclusion that cases where the coolant jet core has similar velocity magnitude to the mainstream flow result in a weak shear layer, a weak counter-rotating vortex pair, and therefore optimal adiabatic effectiveness. Designers can use this information to target the optimal blowing ratio for a given area ratio.

The 12-12-12 and 7-7-7 holes had relatively similar performance at the same blowing ratios and area ratios. The 12-12-12 hole has a lower ejection angle, which keeps the coolant jet close to the endwall and increases lateral spreading. However, due to the larger diffuser and larger expansion angles, the pressure recovery inside the 12-12-12 hole was poor compared to the 7-7-7. This resulted in more over-diffusion and mainstream ingestion, and counteracted the positive benefit of the lowered injection angle. The CFD predicted the poor pressure recovery of the 12-12-12, but did not predict the ensuing over-diffusion, and therefore the CFD predictions for the 12-12-12 adiabatic effectiveness were much higher than the experimental results.

PIV measurements were taken at a downstream plane for the AR2 and AR6 cases, and showed the flowfield differences between a low and high blowing ratio, and low and high area ratio. At the high blowing ratio case of AR2, the jet was detached and exhibited a strong counter rotating vortex pair. Alternately, at the low blowing ratio for AR2, the CRVP was very weak. Consequently, the lower blowing ratio in this case had the highest effectiveness. For the AR6 cases, the CRVP was so weak as to not be observed in the in-plane velocity vectors. These flowfields also confirm that for an increased area ratio, the jet core velocity and mainstream penetration is decreased for a given blowing ratio.

ACKNOWLEDGMENTS

The authors are grateful to Pratt & Whitney, a United Technologies Corp. company, for their generous support of this project. We also would like to thank Phil Irwin for his skilled machining of all of the film cooling holes used in this study.

REFERENCES

[1] Schroeder, R. P., and Thole, K. A., 2014, "Adiabatic Effectiveness Measurements for a Baseline Shaped Film Cooling Hole," ASME Turbo ExpoDüsseldorf, Germany, p. 14.

[2] Bunker, R. S., 2005, "A Review of Shaped Hole Turbine Film-Cooling Technology," Journal of Heat Transfer, 127(4), p. 441.

[3] Goldstein, R. J., and Eckert, E. R. G., 1974, "Effects of Hole Geometry and Density on Three-Dimensional Film Cooling," Journal of Heat and Mass Transfer, 17, p. 13.

[4] Thole, K., Gritsch, M., Schulz, A., and Wittig, S., 1998, "Flowfield Measurements for Film-Cooling Holes With Expanded Exits," Journal of Turbomachinery, 120(2), pp. 327-336.

[5] Peterson, S., and Plesniak, M., 2002, "Short-hole jet-in-crossflow velocity field and its relationship to film-cooling performance," Experiments in Fluids, 33(6), pp. 889-898.

[6] Haven, B. A., and Kurosaka, M., 1997, "Kidney and Anti-Kidney Vortices in Crossflow Jets," Journal of Fluid Mechanics, 352, p. 38.

[7] Gritsch, M., Colban, W., Schär, H., and Döbbeling, K., 2005, "Effect of Hole Geometry on the Thermal Performance of Fan-Shaped Film Cooling Holes," Journal of Turbomachinery, 127(4), pp. 718-725.
[8] Saumweber, C., and Schulz, A., 2012, "Effect of Geometry Variations on the Cooling Performance of Fan-Shaped Cooling Holes," Journal of Turbomachinery, 134(6), p. 16.
[9] Colban, W. F., Thole, K. A., and Bogard, D., 2011, "A Film-Cooling Correlation for Shaped Holes on a Flat-Plate Surface," Journal of Turbomachinery, 133(1), p. 011002.
[10] Kohli, A., and Bogard, D. G., 1999, "Effects of Hole Shape on Film Cooling With Large Angle Injection," ASME International Gas Turbine and Aeroengine Congress.
[11] Kohli, A., and Thole, K. A., "Entrance Effects On Diffused Film-Cooling Holes," Proc. International Gas Turbine & Aeroengine Congress & Exhibition, p. 8.
[12] McDonald, A. T., and Fox, R. W., 1965, "An Experimental Investigation of Incompressible Flow in Conical Diffusers," International Journal of Mechanical Sciences, 8, pp. 125-139.
[13] Klein, A., 1981, "Review: Effects of Inlet Conditions on Conical-Diffuser Performance," Journal of Fluids Engineering, 103, p. 8.
[14] Wolf, S., and Johnston, J. P., 1969, "Effects of Nonuniform Inlet Velocity Profiles on Flow Regimes and Performance in Two-Dimensional Diffusers," Journal of Basic Engineering, 91(3), pp. 462-474.
[15] Leylek, J. H., and Zerkle, R. D., 1994, "Discrete-Jet Film Cooling: A Comparison of Computational Results With Experiments," Journal of Turbomachinery, 116(July 1994), p. 11.
[16] Thole, K. A., Gritsch, M., Schulz, A., and Wittig, S., 1997, "Effect of a Crossflow at the Entrance to a Film-Cooling Hole," Journal of Fluids Engineering, 119(3), pp. 533-540.
[17] Saumweber, C., and Schulz, A., "Comparison the cooling performance of cylindrical and fan-shaped cooling holes with special emphasis on the effect of internal coolant cross-flow," Proc. ASME Turbo Expo 2008: Power for Land, Sea, and Air, American Society of Mechanical Engineers, pp. 893-903.
[18] Coletti, F., Elkins, C. J., and Eaton, J. K., 2013, "An inclined jet in crossflow under the effect of streamwise pressure gradients," Experiments in Fluids, 54(9).
[19] Haydt, S., Lynch, S., and Lewis, S. D., 2016, "The Effect of a Meter-Diffuser Offset on Shaped Film Cooling Hole Adiabatic Effectiveness," ASME Turbo Expo 2016, ASME, Seoul, South Korea, pp. 1-13.
[20] Eberly, M. K., and Thole, K. A., 2013, "Time-Resolved Film-Cooling Flows at High and Low Density Ratios," Journal of Turbomachinery, 136(6), p. 061003.
[21] Figliola, R. S., and Beasley, D. E., 2006, Theory and design for mechanical measurements, John Wiley, Hoboken, N.J.
[22] Schroeder, R. P., and Thole, K. A., 2016, "Effect of High Freestream Turbulence on Flowfields of Shaped Film Cooling Holes," Journal of Turbomachinery, 138, p. 10.